RSC Advances

ROYAL SOCIETY OF CHEMISTRY

www.rsc.org/advances

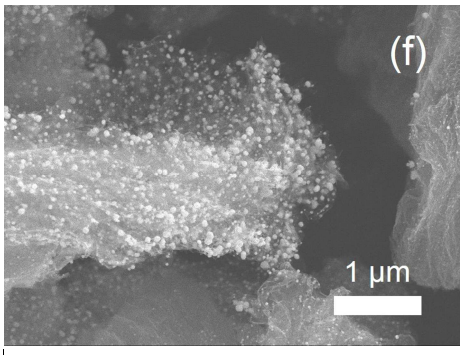

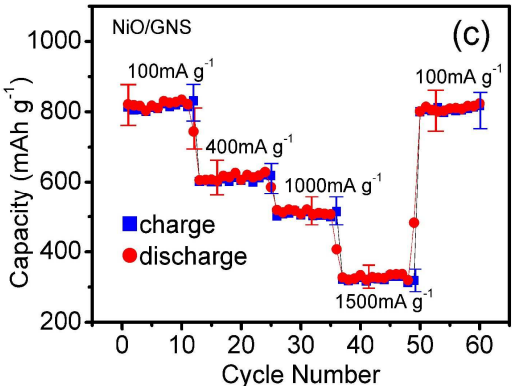

NiO/graphene composite was prepared via an in situ thermal decomposition method. And the composite exhibited high performance as anode material for lithium-ion battery.

Journal Name

RSCPublishing

COMMUNICATION

In situ growth of NiO nanoparticles on graphene as a high-performance anode material for lithium-ion battery anodes with enhanced strain accommodation

Cite this: DOI: 10.1039/x0xx00000x

Received 00th January 2012,
Accepted 00th January 2012
DOI: 10.1039/x0xx00000x
www.rsc.org/

Danfeng Qiu*[a], Gang Bu[a], Bin Zhao[b], Zixia Lin[b]

Nickel oxide (NiO) nanoparticles were directly formed on graphene nanosheets through in situ thermal decomposition of $Ni(NO_3)_2·6H_2O$ and were anchored tightly on the graphene surface. During the charge–discharge process, graphene nanosheets served as a three-dimensional conductive network for the NiO nanoparticles. The lithiation-induced strain was naturally accommodated because of the constraint effect of graphene. Thus, pulverization of NiO nanoparticles was effectively prevented.

Rechargeable solid-state batteries have long been considered as an attractive power source for a wide variety of applications because of their salient features such as high energy density, long stable cycle life, and absence of memory effect [1–3]. In recent years, the use of lithium-ion batteries (LIBs) has expanded into larger scale applications such as hybrid electric vehicles, electric vehicles, and even grid-scale energy storage [4–6]. At present, commercial LIB anode material is typically graphite, which suffers from relatively low theoretical specific capacity of 372 $mAhg^{-1}$ [7], resulting in the limitation of further application of LIBs [8, 9]. Transition metal oxides, such as Co_3O_4 [10], SnO_2 [11], Fe_2O_3 [12], NiO [13, 14], and MoO_2 [15], have been considered as anode materials for LIBs because of their high capacities [16–18]. Among these materials, NiO attracts extensive interest for LIBs because of its low price, nontoxicity, and high theoretical capacity. However, in practical applications, pulverization induced by large volume changes, which leads to loss of electrical contact and subsequent rapid capacity fading, has to be resolved. A common strategy to reduce the volume change is to incorporate NiO with carbonaceous conductive additives such as amorphous carbon [19], carbon nanotubes [20], graphite oxide [21], and graphene [22, 23]. Among these carbon materials, graphene is an excellent substrate to host active nanomaterials for energy applications because of its high conductivity, large surface area, flexibility, mechanical strength, light weight, and chemical stability, which substantially improve lithium ion diffusion kinetics [24]. In the present study, direct anchoring of NiO nanoparticles on graphene nanosheets (GNSs) through a new and versatile in situ thermal decomposition method as LIB anodes is reported. The as-synthesized NiO/GNS nanocomposites could be directly used as LIB electrode without binder or further treatment. The binder-free electrode exhibited high capacity, long cycle life, and excellent rate capabilities as a result of the synergistic effects of the NiO nanoparticles and GNS layers.

Graphite oxide (GO) was synthesized from natural graphite powders (universal grade, 99.985%) according to a modified Hummers method [25]. As-prepared graphite oxide was thermally exfoliated at 300 °C for 3 min in air and subsequently treated at 900 °C for 3 h in Ar. In a typical synthesis of NiO/GNS nanocomposite, 1163.2 mg of $Ni(NO_3)_2·6H_2O$ was mixed with 50 mL of ethanol. A 100 mg portion of GNS was added into the solution and then ultrasonically treated for 10 min. The suspension solution was mixed using a magnetic stirrer in a ventilation cabinet, and the ethanol in the solution evaporated continuously. The dried $Ni(NO_3)_2·6H_2O$ /GNS composite was collected and treated at 200 °C for 10 h in air. $Ni(NO_3)_2·6H_2O$ was transformed into NiO. The relevant mechanism may be illustrated as follows:

$$Ni(NO_3)_2·6H_2O \rightleftarrows NiO+NO_2+O_2+6H_2O \quad (1)$$

The final NiO content in NiO/GNS was approximately 80% by weight. In control experiments, a simple NiO sample was prepared by heating $Ni(NO_3)_2·6H_2O$ at 200 °C for 10 h in air. The obtained samples were investigated via X-ray diffraction (XRD), scanning electron microscopy (SEM), and transmission electron microscopy (TEM). Electrochemical measurements were performed using 2032-type coin cells. Purity was 90 wt% active material and 10 wt% *N*-methylpyrrolidone. The obtained slurry was pasted on a copper foil and dried in vacuum. Coin cells were assembled in an argon-filled glove box using an active material as working electrode, a Li foil as counter electrode, 1 M $LiPF_6$ in ethylene carbonate and diethyl carbonate (1:1 vol), and Celgard 2250 as separator. Charge–discharge measurements were conducted galvanostatically over a voltage range of 0.01 V to 3 V using a battery testing system (LAND, Wuhan Jinnuo Electronics). Furthermore, the tap density of

the electrode is 2 g/cm^3.

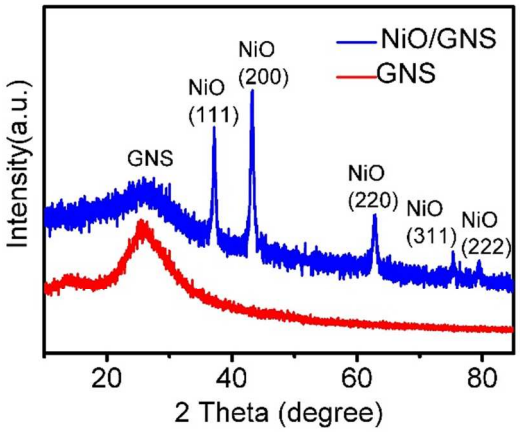

Fig. 1. XRD patterns of the samples.

The XRD patterns of NiO/GNS nanocomposites and NiO particles are shown in Fig. 1. Diffraction peaks at 37.2°, 43.2°, and 62.8° can be respectively indexed to the (111), (200), and (220) NiO crystal given by the standard data (JCPDS file number 40-1467). The broad peak at approximately 25 °C was the diffraction peak from the multilayer graphene of the GNS sample.

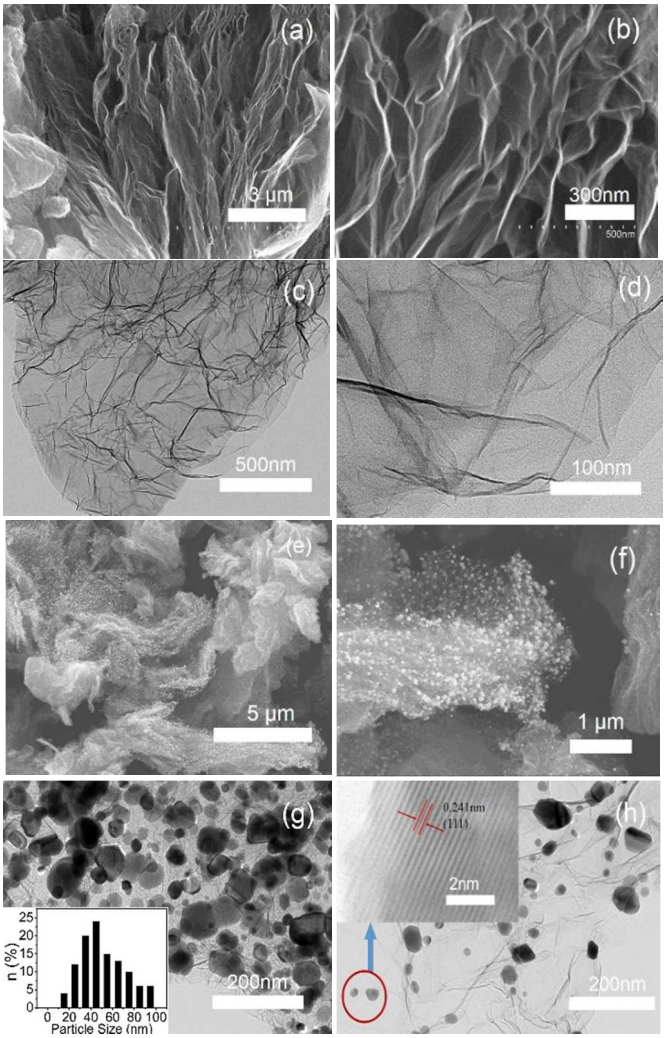

Fig. 2. SEM (a and b) and TEM (c and d) images of GNS; SEM(e and f) and TEM (g) images of NiO/GNS Inset: particle size distribution of NiO nanoparticles; High resolution TEM (h) images of NiO/GNS.

The morphologies of as-prepared GNS and NiO/GNS were examined by SEM and TEM. The typical SEM and TEM images of the GNS sample are shown in Figs. 1a to 1d. The GNS sample exhibited a nanosheet structure resulting from the decomposition of the oxygen-containing groups of GO during thermal exfoliation process [26]. In particular, the SEM images show numerous macropores among the nanosheets. These macropores facilitate the combination of $Ni(NO_3)_2 \cdot 6H_2O$ and GNS. The SEM images of NiO/GNS under different magnifications are presented in Figs. 2e and 2f. NiO nanoparticles with diameters ranging from 10 nm to 100 nm integrated tightly with GNS. The TEM images of NiO/GNS are presented in Figs. 2g and 2h, revealing the firm attachment of NiO nanoparticles to GNS even after ultrasonication treatment to disperse the sample for TEM observation. As shown in Fig. 2(g), the particle size of NiO nanoparticles was determined to be about 40 ± 5 nm after measuring 100 particles. High-resolution TEM was also performed to confirm the interaction between NiO nanoparticles and the GNS layers of the as-synthesized NiO/GNS nanocomposites. In Fig. 2(h), lattice fringes with spacing of 0.241 nm correspond to interplanar spacing of the (111) crystal plane of monoclinic NiO.

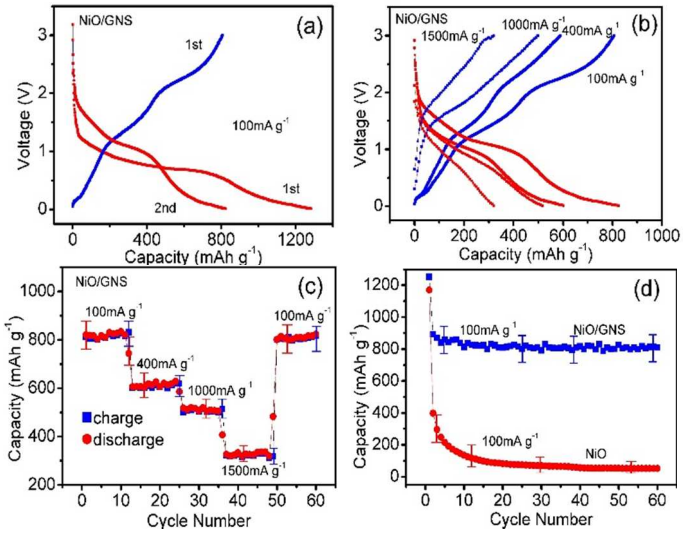

Fig. 3. (a) Discharge and charge curves of NiO/GNS for the first and second cycles at a current density of 100 mA g^{-1}; (b) representative charge and discharge curves of MnO/GNS at various current densities; (c) capacity retention of NiO/GNS at various current densities; and (d) discharge capacity retention of NiO/GNS and simplex NiO at a current density of 100 mA/g.

The electrochemical properties of bulk NiO and as-prepared NiO/GNS nanocomposite electrode were investigated by CV over a range of 0.01 V to 3.0 V, as shown in Fig. 3. The charge and discharge curves of the NiO/GNS electrode run for one and two cycles at 100 mAg^{-1} are shown in Fig. 3a. The first discharge curve of NiO/GNS shows a voltage plateau at approximately 0.7 V. During the second circle, a rapid drop in potential to about 1.1 V is observed, followed by a long voltage plateau between 1.1 V and 0.7 V. This voltage plateau results from two reactions, one of which is

the conventional reaction of NiO [27], which is expressed as follows:

$$NiO + 2Li \rightleftarrows Ni + Li_2O \quad (2)$$

The other originates from the reaction of GNS with Li. The representative charge and discharge curves of NiO/GNS at various current densities are presented in Fig. 3b. With the increase in current density, the charge potential of GNS/NiO increased and the discharge potential decreased, rendering higher overpotential. The cell was first cycled at a low current density of 100 mAg^{-1} for 10 cycles, where a stable specific capacity of approximately 800 $mAhg^{-1}$ (Fig. 3c) was obtained. The capacity was as high as 600 $mAhg^{-1}$ after the current density was increased four times, a value that was still higher than the theoretical capacity of graphite (372 $mAhg^{-1}$). Even at a high current density of 1,500 mAg^{-1}, more than 40% of the capacity can be retained. A capacity of approximately 800 $mAhg^{-1}$ was retained after 50 cycles of charge and discharge at various current densities (Fig. 3c), indicating good cycling stability.

The charge/discharge capacity curves of electrodes fabricated from NiO/GNS versus the cycle number under a charge/discharge current density of 100 $mAhg^{-1}$ at 25 °C are shown in Fig. 3d. The specific discharge capacity of the NiO/GNS composite is approximately 800 $mAhg^{-1}$, or about twice that of graphite, even after 60 cycles. In the case of pure NiO, under a charge/discharge current density of 100 mAg^{-1}, only 50 $mAhg^{-1}$ was retained by the electrode after 60 cycles. This result indicates that graphene-loaded NiO nanoparticles feature improved cycling stability. NiO nanoparticles were integrated tightly with GNS. The flexible GNS provided high electrical conductivity throughout the electrode and served as a mechanically strong framework. Under the constraining effects of the GNS at the molecular level, the volume expansion/contraction of cobalt oxides during the lithium insertion/extraction process progresses along the vertical direction of the GNS. As a result, the nanocomposite presented a large lithium storage capacity, excellent cyclic stability, and good rate capability. The results show a promising method for the synthesis of graphene-based nanocomposites and an interesting nanostructured system for LIB electrode materials that undergo large volume changes during cycling.

Conclusions

In summary, a facile method to synthesize NiO/GNS composites was developed. The synthesis strategy was based on a one-step in situ growth of NiO nanoparticles on a grapheme matrix and provided a simple, low-cost, and effective method of preparing NiO/GNS composites because no additional chemicals were necessary during synthesis. NiO nanoparticles were uniformly distributed and anchored on the surface of GNS layers. The binder-free electrodes exhibited excellent electrochemical performance as LIB anode material. We expect that this process can be further explored to produce binder free electrodes of other graphene/metal-oxide composites with high performance for application in energy storage devices.

Acknowledgements

This work was supported by the National Natural Science Foundation of China (Nos. 51202106, 61076017, and 60928009), the Fundamental Research Funds for the Central Universities (No. 1127021010), and 973 Project (Grant No. 2013CB932900).

Notes and references

[a]Key Laboratory of Radar Imaging and Microwave Photonics (Nanjing Univ. Aeronaut. Astronaut.), Ministry of Education, College of Electronic and Info rmation Engineering, Nanjing University of Aeronautics and Astronautics, N anjing, 210016, China E-mail: dfqiu@nuaa.edu.cn; Tel./fax: 86-25-84892452
[b] National Laboratory of Microstructures and School of Electronic Science and Engineering, Nanjing University, Nanjing, China

1 K. Kang, Y. S. Meng, J. Breger, C. P. Grey and G. Ceder, *Science*, 2006, 311, 97.
2 Y. Yao, M. T. McDowell, I. Ryu, H. Wu, N. A. Liu, L. B. Hu, W. D. Nix and Y. Cui, *Nano Lett*., 2011, 11, 2949.
3 K. Amine, I. Belharouak, Z. Chen, T. Tran, H. Yumoto, N. Ota, S. T. Myung and Y. K. Sun, *Adv. Mater*., 2010, 22, 3052.
4 J. Yan, A. Sumboja, E. Khoo and P. S. Lee, *Adv. Mater.*, 2011, 23, 746.
5 S. Guo and S. Dong, *Chem. Soc. Rev.*, 2011, 40, 264.
6 L. Shen, X. Zhang, E. Uchaker, C. Yuan and G. Cao, *Adv. Energy. Mater.*, 2012, 2, 691.
7 J. Liu, Y. Li, H. Fan, Z. Zhu, J. Jiang, R. Ding, Y. Hu and X. Huang, *Chem. Mater.*, 2010, 22, 212.
8 Z. Wang, D. Luan, S. Madhavi, Y. Hu and X. W. Lou, *Energy Environ. Sci.*, 2012, 5, 5252.
9 J. Li, Y. Zhao, Y. Ding and L. Guan, *RSC Adv.*, 2012, 2, 4205.
10 W. Y. Li, L. N. Xu,and J. Chen, *Adv. Funct. Mater.*, 2005, 15, 851.
11 Y. M. Li, X. J. Lv, J. Lu , J. H. Li, *J. Phys. Chem. C*, 2010, 114, 21770.
12 M. B. Zheng, D. F. Qiu, B. Zhao, L. Y. Ma, X. R. Wang, Z. X. Lin, L. J. Pan, Y. D. Zheng and Y. Shi, *RCS Adv.*, 2013, 3, 699.
13 X. Wang, H. M. Mao and Y. C. Shan, *RCS Adv.*, 2014, 4, 35614.
14 Y. J. Mai, S. J. Shi, D. Zhang, Y. Lu, C. D. Gu, J. P. Tu, *J. Power Sources*, 2012, 204, 155.
15 Z. X. Huang, Y. Wang, Y. G. Zhu, Y. M. Shi, J. I. Wong and H. Y. Yang, *Nanoscale*, 2014, 6, 9839
16 P. Poizot, S. Laruelle, S. Grugeon, L.Dupont and J.-M. Tarascon, *Nature*, 2000, 407, 496.
17 P. L. Taberna, S. Mitra, P. Poizot, P. Simon and J.-M. Tarascon, *Nat. Mater.*, 2006, 5, 567.
18 X. W. Lou, D. Deng, J. Y. Lee, J. Feng and L. A. Archer, *Adv. Mater.*, 2008, 20, 258.
19 L. X. Liu, H. Guo, J. J. Liu, F. Qian, C. H. Zhang, T. T. Li, W. W. Chen, X. J. Yang and Y. C. Guo, *Chem. Commun*, 2014, 50, 9485.
20 C. H. Xu, J. Sun and L. A. Gao, *J. Power Sources*, 2011, 196, 5138
21 Zhou, H. Song, L. Ma and X. Chen, *RSC Adv.*, 2011, 1, 782.
22 S. Yang, X. Feng, S. Ivanovici and K. Mullen, *Angew. Chem., Int. Ed.*, 2010, 49, 8408.
23 S. Bai and X. Shen, *RSC Adv.*, 2012, 2, 64.
24 H.Wang, L.-F. Cui, Y. Yang, H. S. Casalongue, J. T. Robinson, Y. Liang, Y. Cui and H. Dai, *J. Am. Chem. Soc.*, 2010, 132, 13978.
25 W. S. Hummers,and R. E. Offeman, *J. Am. Chem. Soc.*, 1958, 80, 1339.
26 Q. L. Du,M. B. Zheng, L. F. Zhang, Y. W.Wang, J. H. Chen, L. P. Xue, W. J. Dai, G. B. Ji and J. M. Cao, *Electrochim. Acta*, 2010, 55, 3897.